Chapter 5
Characterization of Self-Healing Phenomena on Micro- and Nanoscale Level

This chapter describes and discusses some of the characterization methods employed to verify the physical and chemical aspects of self-healing on the micro- and nanoscale levels. These methods are used to confirm that the healing agents are encased and released from nanofibers (NFs), spread, reacted, and solidified. The methods discussed in this section are also used to elucidate the morphological changes in the damaged material caused by the released healing agents. Characterization methods including visualization (Sect. 5.1), spectroscopy (Sect. 5.2), and thermal analysis (Sect. 5.3) are discussed below.

5.1 Visualization

To ensure that the healing materials are encapsulated in the fiber cores, defect-free and bead- or blob-free uniform fibers are preferred. The overall morphologies of fibers containing healing agents can be inspected using optical microscopy (OM, Sett et al. 2015), scanning electron microscopy (SEM, An et al. 2014), atomic force microscopy (AFM, Sinha-Ray et al. 2013), and optical profilometry (Ghosal et al. 2016). However, only the exterior features can be observed by these methods. The core-shell architecture is one of the most important structural features of self-healing fibers. Thus, the presence of a core filled with a healing agent must be confirmed using transmission electron microscopy (TEM), which allows for imaging through sufficiently thin shells (An et al. 2015; Lee et al. 2015). Fluorescence imaging can also be used to observe the encased core material if it is blended with a fluorescent dye or contains fluorescent markers (Sinha-Ray et al. 2011; Pang and Bond 2005a, b). The internal damage incurred within a composite can be investigated using ultrasonic C-scanning or X-radiography (Bleay et al. 2001; Pang and Bond 2005a, b). NF images obtained using the methods described in this chapter are shown in Fig. 5.1. It should be emphasized that Fig. 5.1 illustrates the observation methods, with not necessarily core-shell fibers containing healing agents (some fibers in Fig. 5.1 are not of this

A. L. Yarin et al., *Self-Healing Nanotextured Vascular Engineering Materials*, Advanced Structured Materials 105, https://doi.org/10.1007/978-3-030-05267-6_5

type). A number of additional SEM, TEM and fluorescent images of core-shell NFs filled with healing agents can be found in Chaps. 1 and 4.

5.2 Spectroscopic Characterization

The elemental composition of the released healing agents can be analyzed using energy-dispersive X-ray spectroscopy (EDX). For example, the presence of dimethyl siloxane resin monomer (C_2H_6OSi, DMS; cf. Sect. 2.2) in the core encapsulated in the polyacrylonitrile [$(C_3H_3N)_n$, PAN] shell of core-shell NFs was confirmed by EDX analysis. The spectrum of the NFs contained a distinct peak related to silicon (Si) at the Kα value of ~1.8 keV (see Fig. 5.2) (Lee et al. 2014b, 2015).

The presence of a curing agent (dimethyl-methyl hydrogen-siloxane, DMHS) within NFs formed by emulsion electrospinning (Sect. 4.3) was confirmed by EDX in Lee et al. (2014b). Figure 5.3 compares SEM images and the EDX data for the uniform parts of NFs and in the beads on the fibers. The beads should contain more curing agent, as they are bulkier sections with more space to store the curing agent. Figure 5.4 confirms the greater amount of curing agent in the beads on the fibers through a comparison of the silicon contents in different detection domains corresponding to Spectra 3 and 4. The peak corresponding to the silicon content is higher for the bead on the fibers. Silicon is also detected in the uniform parts of these fibers, indicating continuous curing agent cores throughout these core-shell NFs. It should be emphasized that the curing agent is uniformly distributed in the cores of multiple long sections of NFs spanning the beads. Therefore, a 3D network of such NFs allows uniform coverage of the surface, which is hard to achieve with an approach involving capsules.

In Sinha-Ray et al. (2012), EDX was employed to detect healing agents of dicyclopentadiene (DCPD; cf. Sect. 2.1) or isophorone diisocyanate (cf. Sect. 2.3) in the fiber cores. The fibers were formed using co-electrospinning, emulsion electrospinning, and coaxial solution blowing described in Sects. 4.2, 4.3 and 4.5, respectively. The quantification of light elements by EDX is extremely difficult and may be inaccurate because of the absorption of low-energy X-rays in a specimen, in the detector window and the silicon dead layer. In addition, to avoid any possible interference, samples cannot be sputter-coated with metal. Therefore, samples should be inspected in a differential-pressure SEM chamber, which employs gas ions to neutralize the electric charge. This causes the beam to widen, which can introduce difficulties with localization for any analysis conducted. This widening can begin from a submicrometer-sized spot in an ultra-high vacuum SEM to a spot of ~100 μm in a differential-pressure SEM (in addition to the possible movement of the NF mat under an electron beam).

When EDX is employed, materials are characterized based on their Kα energy shell. In the core-shell NFs studied by Sinha-Ray et al. (2012), the shell consisted of PAN and the core comprised either DCPD ($C_{10}H_{12}$) or isophorone diisocyanate ($C_{12}H_{18}N_2O_2$). In the PAN/DCPD core-shell system, it was implied that the EDX

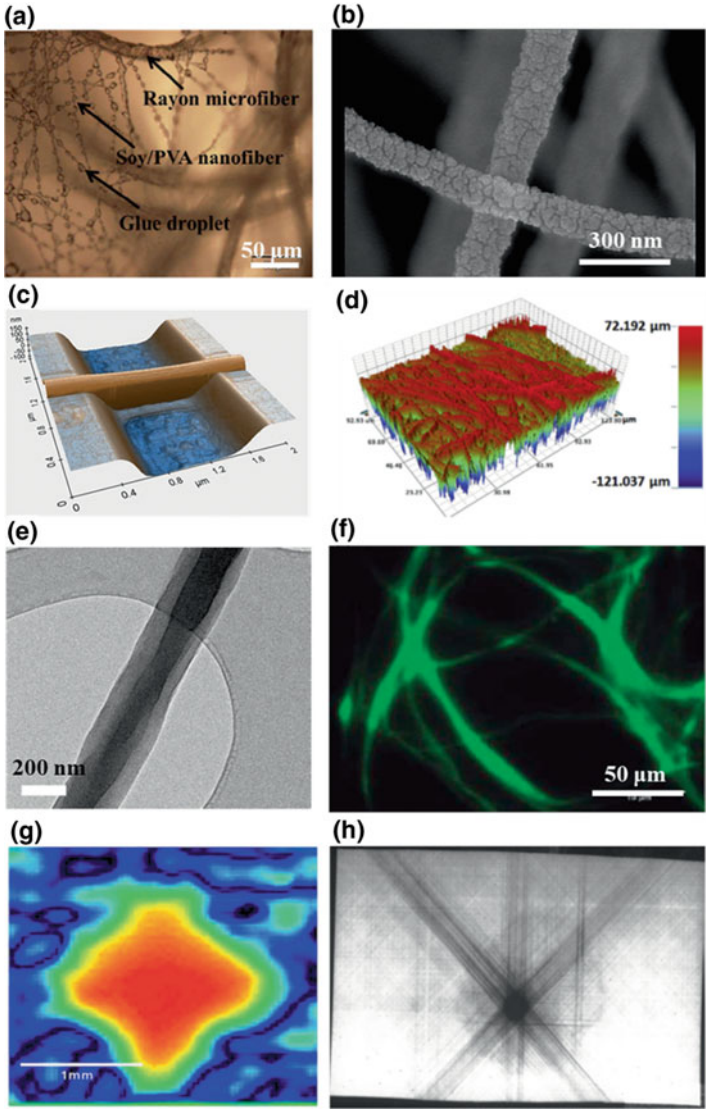

Fig. 5.1 **a** OM image of as-deposited soy protein/poly(vinyl alcohol) (PVA) NFs on a rayon pad. Reprinted with permission from Sett et al. (2015). **b** SEM image of electrospun polyacrylonitrile (PAN) NFs sputter-coated by platinum. Reprinted with permission from An et al. (2014). **c** AFM landscape-mode image of nylon-6 fiber deposited over a trench. Reprinted with permission from Sinha-Ray et al. (2013). **d** Optical profilometry image. Reprinted with permission from Ghosal et al. (2016). **e** TEM image of resin monomer (core)-PAN (shell) NF; cf. Fig. 4.9 in Sect. 4.2. Reprinted with permission from An et al. (2015). **f** Fluorescence microscopy image of fibers of nylon-6/soy protein blend. Reprinted with permission from Sinha-Ray et al. (2011). **g** Ultrasonic C-scanning image after impact damage at the impact energy of 0.8 J (i.e., indentation at 1400 N). Reprinted with permission from Pang and Bond (2005b). **h** X-radiograph of quasi-isotropic hollow glass/fiber composite after impact test obtained using opaque X-ray dye incorporated within the impact region. Reprinted with permission from Bleay et al. (2001)

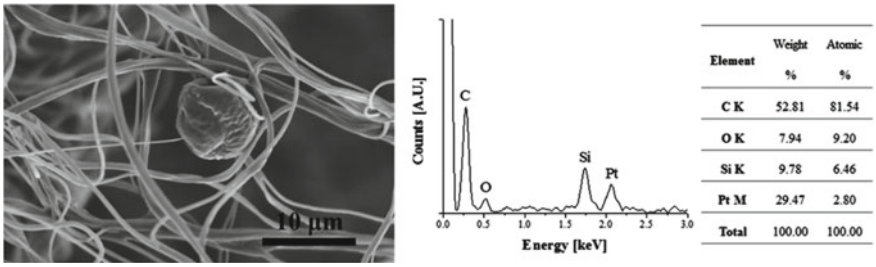

Element	Weight %	Atomic %
C K	52.81	81.54
O K	7.94	9.20
Si K	9.78	6.46
Pt M	29.47	2.80
Total	100.00	100.00

Fig. 5.2 SEM image of a spherical mass of DMS resin monomer released from damaged co-electrospun NFs (cf. Fig. 4.6d in Sect. 4.2) and EDX analysis results for this mass. Reprinted with permission from Lee et al. (2015)

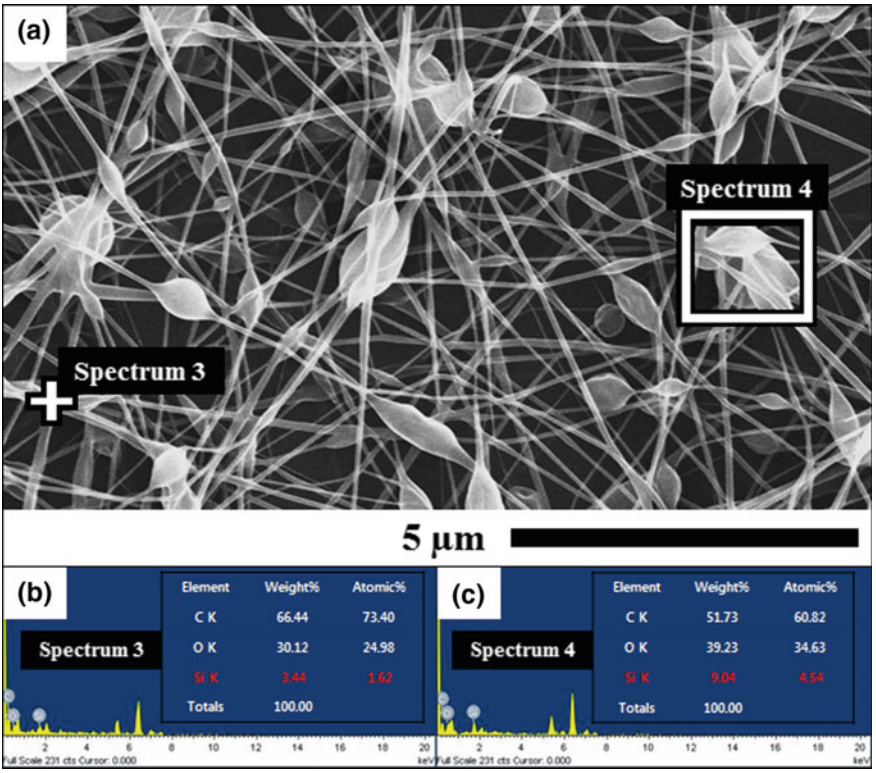

Fig. 5.3 **a** SEM and **b**, **c** EDX data for NFs formed by the emulsion electrospinning with curing agent in the cores. Data were obtained in **b** the region of a uniform fiber, Spectrum 3, and in **c** the region of a bead on the fiber, Spectrum 4. Reprinted with permission from Lee et al. (2014b)

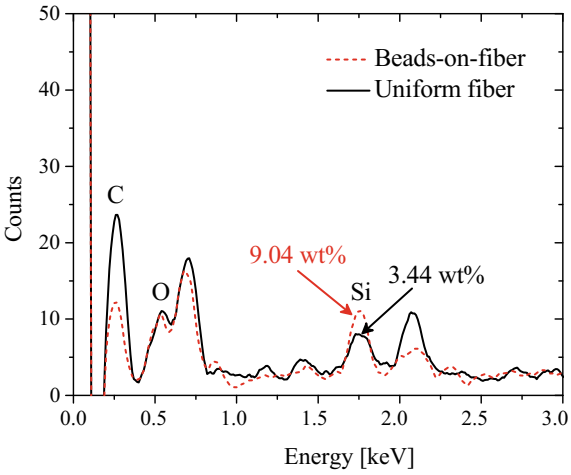

Fig. 5.4 EDX data for core-shell NFs with curing agent in the core. A silicon peak at 1.739 keV implies the presence of curing agent withing NFs. Reprinted with permission from Lee et al. (2014b)

spectrum of the DCPD core, which contained little or no nitrogen, should be easily distinguishable from the shell spectrum, which contained nitrogen. A careful observation of the EDX series revealed that carbon and nitrogen corresponded to the Kα value of 0.277 keV and 0.392 keV, respectively. The energy resolution of the detector was ~0.140 keV, meaning that, in the EDX spectrum, the peaks of nitrogen and carbon would overlap, impeding reliable characterization based on the presence or absence of nitrogen. Indeed, it is shown in Fig. 5.5a and b for the PAN/DCPD core-shell fibers that the nitrogen peak is completely obscured by the neighboring carbon peak, thus making it impossible to prove the existence of DCPD in the core by EDX. However, the spectrum of a cross-section of PAN/isophorone diisocyanate NFs (Fig. 5.5c) is more informative. Figure 5.5c shows that the oxygen peak in the core in such fibers is much higher (~8%; Fig. 5.5c) than that in the shell (~3%; Fig. 5.5a). This indicates the presence of isophorone diisocyanate in the fiber core. However, the difference in the oxygen peaks is not very pronounced, and the comparison of Fig. 5.5a and c is more qualitative than quantitative.

An additional question arises in relation to the released healing agents: whether they mix, polymerize, and solidify, or remain unmixed and liquid. Solidification does not occur in any individual fiber core alone because the cores contain either DMS resin monomer or the curing agent in separate fibers, as in Lee et al. (2017a). Solidification occurs only when the healing agents are released from the ruptured fiber cores, mixed, and polymerized. It should be emphasized that neither X-ray diffraction (XRD), EDX, nor Raman spectroscopy can determine whether a mixed drop containing both resin monomer and curing agent is polymerized, and thus solidified. This can be determined only by observing the change in the surface texture of a drop, as was shown in Sect. 3.3; cf. Figs. 3.21 and 3.22. Such a change can also be noted via a detailed inspection of the images like those in Fig. 5.6, demonstrating that polymerization and solidification occurred in the drops shown.

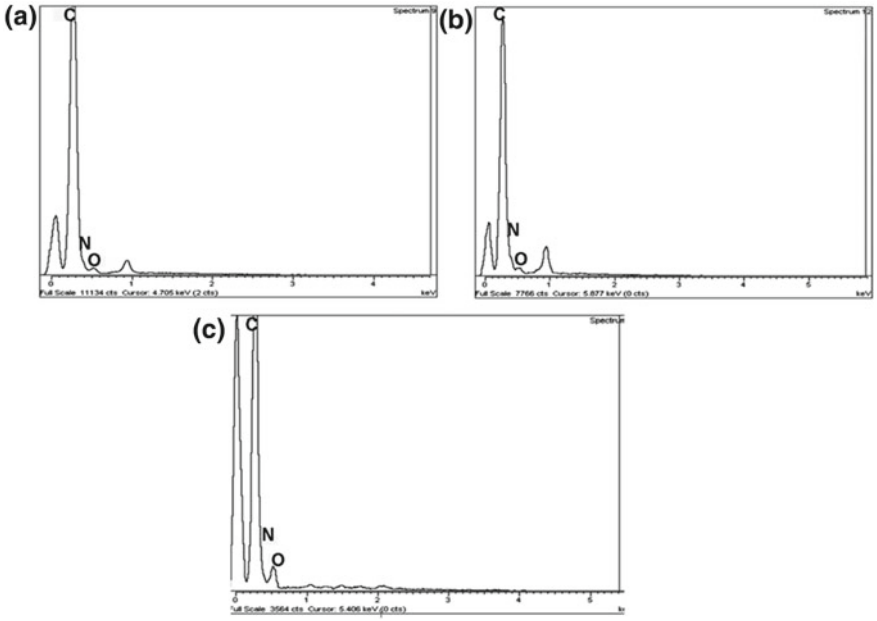

Fig. 5.5 EDX spectra of **a** NF shell (PAN), and **b** a cross-section of PAN/DCPD NF. The presence of nitrogen is masked by the neighboring carbon peak in the spectrum because of the energy resolution of the detector. Panel **c** shows a cross-sectional EDX spectrum of a PAN/isophorone diisocyanate NF. Panel **c** reveals a visible increase in the oxygen peak compared to that in panel **a**. This rise is attributed to the presence of the oxygen-containing isophorone diisocyanate in the fiber core. Reprinted with permission from Sinha-Ray et al. (2012)

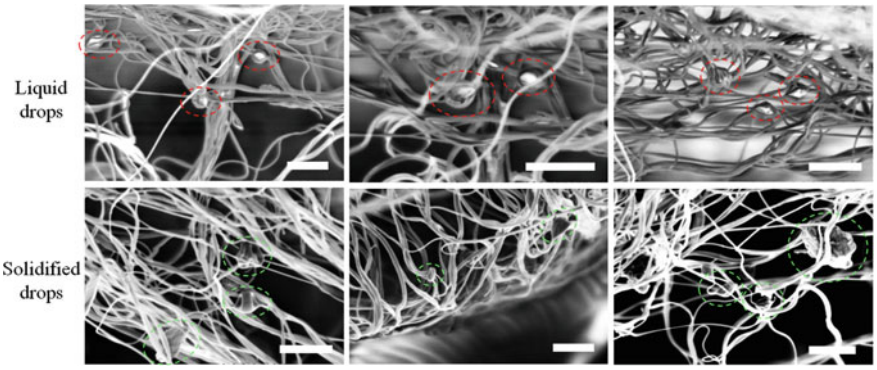

Fig. 5.6 SEM images of cut zone in a PRC (PAN–resin-curing agent) nanofiber mat (scale bars are 5 μm). The surrounding vacuum could have facilitated drop release from the fibers; however, such a release was also observed in open air under ambient pressure and temperature in An et al. (2015). Reprinted with permission from Lee et al. (2017a)

Fourier-transform infrared (FTIR) and Raman spectroscopies performed at room temperature in open air can also be used as nondestructive imaging techniques. The healing process, that is, the polymerization of the released healing agents, can be investigated using these techniques (Zanjani et al. 2015, 2017; Yerro et al. 2016). For example, in the case of DCPD, the bands at wavenumbers of 1572 cm^{-1} and 1614 cm^{-1} are assigned to the $\nu(C = C)$ stretching vibrations of the DCPD monomer (see Fig. 5.7). The occurrence of the healing process is confirmed by the fact that the disappearance of the peak at 1572 cm^{-1} and the red-shifting of the peak at 1614 cm^{-1}, which suggest the polymerization of DCPD (Yerro et al. 2016). FTIR analysis has also been used to confirm the encapsulation of hardener and epoxy within a fiber structure. Figure 5.7c and d show the FTIR spectra of hardener and resin, respectively. The peak at 1592 cm^{-1} corresponds to N–H bending vibrations, while the strong peak at 1150 cm^{-1} is related to the stretching of C–N bonds, confirming the presence of the amine-based hardener in the fiber structure (Fig. 5.7c). Furthermore, the peaks at 815 and 840 cm^{-1}, which belong to the oxirane groups, verify the presence of the epoxy resin within the triaxial fiber structure formed in Zanjani et al. (2015) (Fig. 5.7d).

Raman spectroscopy is another method used to determine the chemical compositions of specific healed or unhealed regions in self-healing materials. The Raman spectrum of PDMS in the healed crack studied by Lee et al. (2017b), mentioned in Sect. 3.4, was used to confirm that the resin and curing agent were released and that the resin was cured on the PDMS surface of the surrounding matrix. The bonds in the PDMS molecule, namely the Si–O–Si, Si–C, and CH_3 bonds, exhibit peaks at the wavenumbers of 492 cm^{-1}, 618/712 cm^{-1}, and 1265 cm^{-1}, respectively, in the Raman spectrum of PDMS (Jayes et al. 2003). The spectral peaks for the resin monomer, curing agent, and dyes used (cf. Fig. 3.25), and their corresponding wavenumbers are listed in Table 5.1. The peaks were selected to distinguish between the released resin monomer and curing agent on the cured PDMS surface. In particular, the resin monomer/curing agent mixing zone was investigated to confirm that mixing and curing had occurred successfully. The peaks at 1541 cm^{-1} (⁎) and 2168 cm^{-1} (⬥) seen in the spectra of the resin monomer (Fig. 5.8b) and the curing agent (Fig. 5.8c) are not seen in the spectrum of cured PDMS (Fig. 5.8a). These two peaks, which correspond to the CH_2–NH–CH_2 and Si–H bonds, respectively, disappear as the resin monomer is polymerized by the curing agent (Colthup et al. 1975). In addition, the dyed resin monomer and curing agent exhibit additional peaks (○ and ●), which correspond to the pigments used to color them. The Raman spectrum of the mixing zone exhibits the peaks described above. The mixing zone is also shown in the optical image in Fig. 5.9, marked (f). The Raman spectrum does not contain the peaks at 1541 cm^{-1} (⁎) and 2168 cm^{-1} (⬥) seen from the uncured resin monomer and curing agent; thus, it is considered to correspond to the cured PDMS. It does contain peaks related to both the dyed resin (○) and the curing agent (●) released from the damaged channels (cf. Fig. 3.25 in Sect. 3.4). This proves that the material in the mixing zone is cured PDMS formed by the mixing of the resin monomer and the curing agent released from the damaged channels and their subsequent polymerization on the crack banks (see Fig. 3.28 in Sect. 3.4).

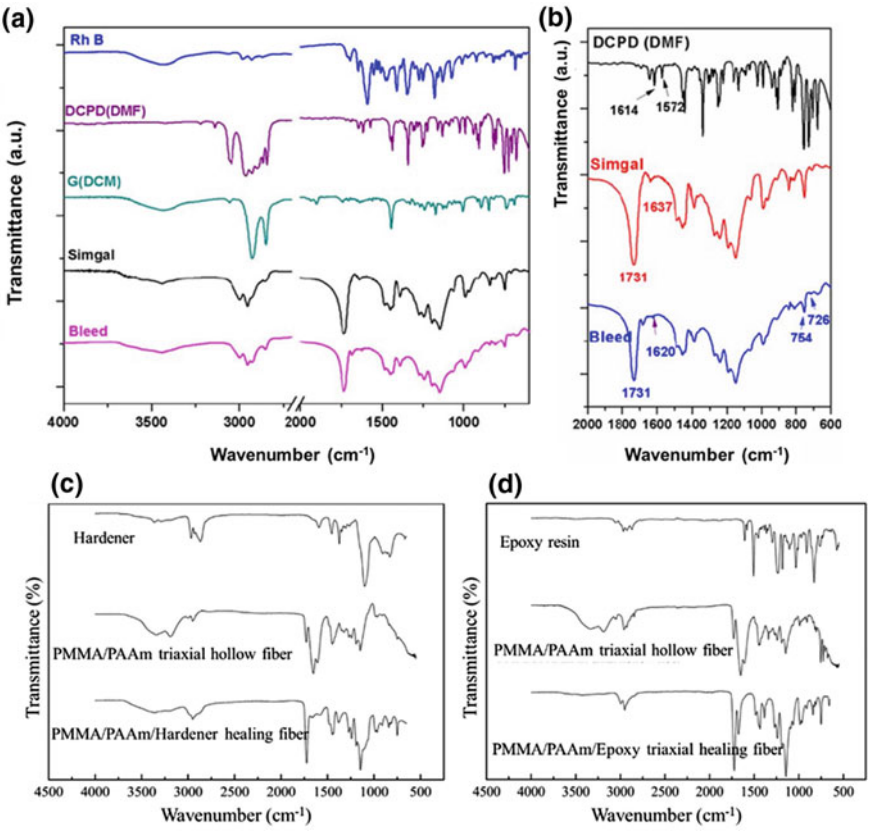

Fig. 5.7 **a** FTIR spectra of the initial materials and self-healing bleed. RhB: Rhodamine B; DCPD(DMF): 10 wt% DCPD solution in DMF; G(DCM): 1 wt% Grubbs' catalyst solution in methylene chloride (DCM); poly(DCPD) (RhB): ROMP (ring-opening metathesis polymerization) of polymer DCPD with RhB. **b** Spectra of DCPD(DMF), Simgal (a drug), and the bleed. Reprinted with permission from Yerro et al. (2016). **c** FTIR spectra of hardener, poly(methyl methacrylate)/poly(acrylamide) (PMMA/PAAm) triaxial hollow fibers, and PMMA/PAAm/hardener triaxial fibers. **d** FTIR spectra of epoxy resin, PMMA/PAAm triaxial hollow fibers, and PMMA/PAAm/epoxy triaxial fibers. Reprinted with permission from Zanjani et al. (2015)

Surface images from the same location of the microchannel system (in the mixing zone) are obtained using OM and analyzed using an optical surface profiler (see Fig. 5.9a and b, respectively; cf. Sect. 5.1). The pebble-like mixing zone between the two channel ends is clearly visible in Fig. 5.9a. The estimated height of this pebble-like zone is approximately 25 μm, according to the profilometry data.

Accordingly, it was found that in the macroscopic experiment of Lee et al. (2017b), the resin monomer and curing agent released into a crack were mixed and cured to

Table 5.1 Wavenumbers corresponding to the peaks seen in the Raman spectra

Wavenumber (cm^{-1})	Assignment
492	Si–O–Si symmetric stretching
618, 712	Si–C symmetric stretching
2907	CH_3 symmetric stretching
2965	CH_3 asymmetric stretching
1541 (∗)	marker for resin
2168 (⬥)	Marker for cure
1184, 1490 (○)	Marker for dye (resin)
1215, 1448 (●)	Marker for dye (cure)

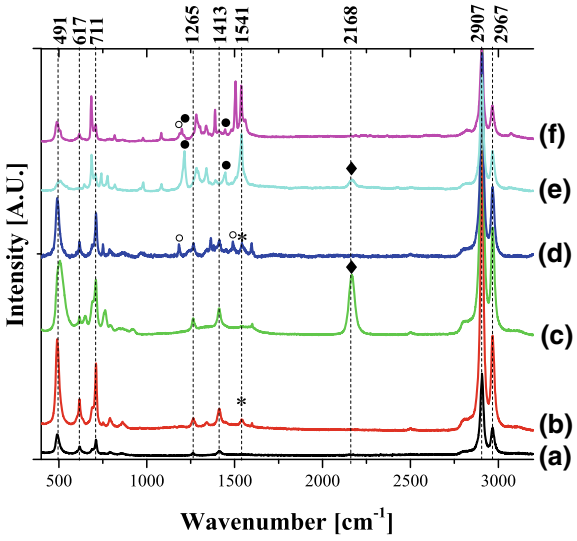

Fig. 5.8 Raman spectra: **a** cured PDMS, **b** pure resin monomer (∗), **c** pure curing agent (⬥), **d** dyed resin (○), **e** dyed curing agent (●), **f** mixing zone (the optical image is shown in Fig. 5.9a). Reprinted with permission from Lee et al. (2017b)

form additional PDMS chunks that helped to heal or stitch the crack banks together (cf. Fig. 3.28 in Sect. 3.4).

In addition, the self-healing of bisphenol A (BPA)-based epoxy resin was also studied using Raman spectroscopy in Patrick et al. (2014). The resin and hardener exhibited peaks at 1256 cm^{-1} (oxirane ring)/1610 cm^{-1} (phenyl ring) and 1656 cm^{-1} (amide-I), respectively (data is not shown here) (Farquharson et al. 2002; Merad et al. 2009; Maiti et al. 2004). Thus, based on the Raman spectrum of the fracture surface, the delivery of the healing agent and the occurrence of the healing (mixing and polymerization) processes were confirmed.

5.3 Thermal Analysis

Thermogravimetric analysis (TGA) and differential thermogravimetry (DTG) are useful in confirming the encapsulation of the self-healing cores in NF shells. Using these thermal analysis methods, the phase-change temperature can be determined (e.g., the melting or evaporation points). The change in the weight owing to the release of substantial amount of volatile substances or gasification during the phase-change process can be determined through TGA. DTG shows the first derivative of the weight-loss curve obtained by TGA and indicates the temperatures corresponding to the phase changes. According to the previous studies (Lee et al. 2014a, b; An et al. 2015), the evaporation temperatures of DMS resin monomer and its curing agent (uncured) are 576.3 °C (●) and 176.1 °C (⬥), respectively, while that of PAN is

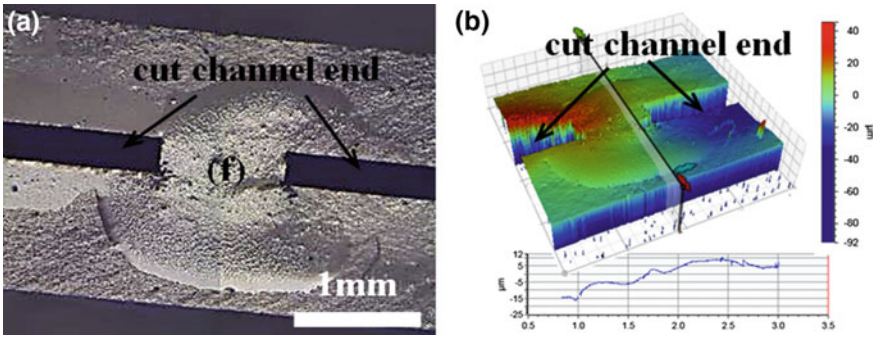

Fig. 5.9 **a** Optical image of cut surface (crack) on the microchannel system (cf. Figs. 3.25 and 3.28 in Sect. 3.4). **b** Optical profilometry image of the surface. Note that the spreading of the released healing agents is fully dominated by wettability, and they spread in all directions, including against gravity. Reprinted with permission from Lee et al. (2017b)

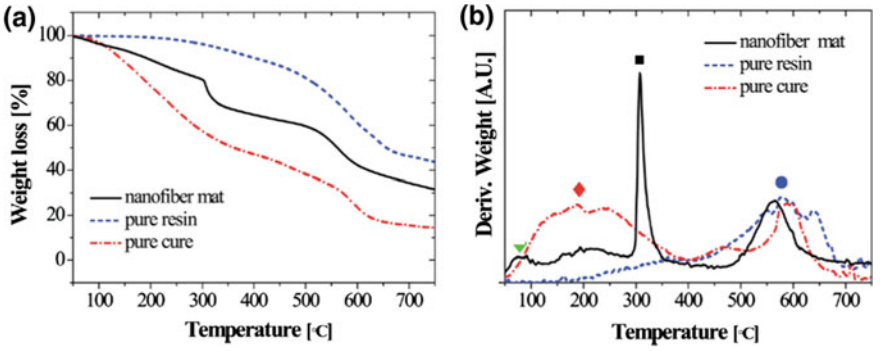

Fig. 5.10 Thermal analysis of core-shell NFs. **a** TGA curves of the core materials (DMS resin monomer and curing agent) and NF mat containing these materials within the cores. **b** DTG curves. The NF mat containing healing agents in the fiber core was obtained by emulsion electrospinning (cf. Sect. 4.3). Reprinted with permission from Lee et al. (2014a)

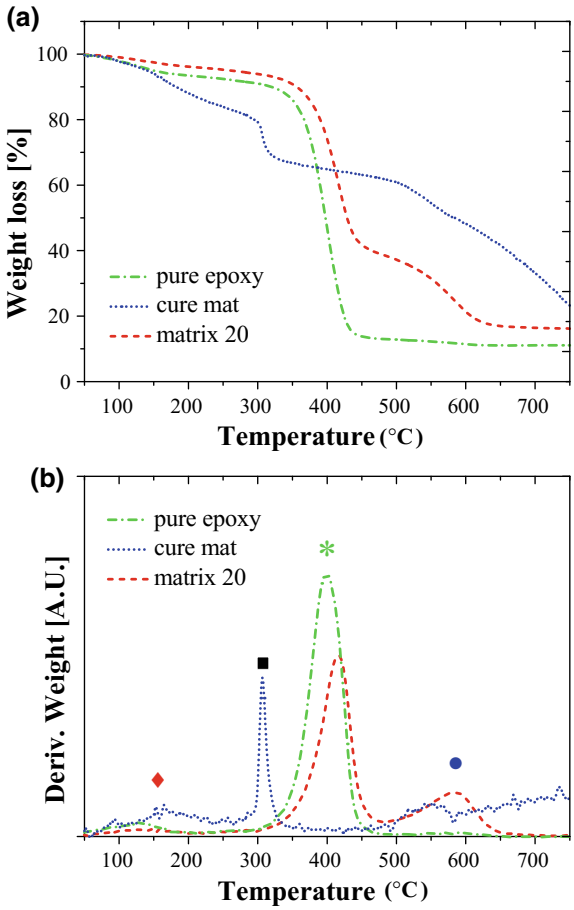

Fig. 5.11 **a** TGA results. **b** The corresponding DTG results. (◆ curing agent 176.1 °C, ■ PAN 305.0 °C, * epoxy–resin matrices with 20 wt% of resin monomer 416.1 °C, ● resin monomer 576.3 °C). Note that "matrix 20" herein refers to the epoxy–resin matrices with 20 wt% of resin monomer. The NF mat with curing agent in the fiber cores is denoted as "cure mat" herein. The NF mat containing curing agent in the fiber cores was obtained by emulsion electrospinning (cf. Sect. 4.3). Reprinted with permission from Lee et al. (2014a)

305.0 °C (■) (see Fig. 5.10, with the data for a fully vascular NF mat incorporating two mutually entangled networks of core-shell NFs containing either resin monomer or curing agent in the cores; cf. Sect. 4.3).

The results of the TGA of the hybrid self-healing materials (see Sect. 4.3) in Lee et al. (2014b) are presented in Fig. 5.11. The peak at 176.1 °C revealed by the NF mat corresponds to the curing agent, which is substantiated by a clearly distinct peak at ~305 °C, corresponding to PAN, agreeing with the results shown in Fig. 5.10. Indeed, 176.1 °C is the boiling temperature of the curing agent. In these materials, the epoxy matrices contained 5 wt% and 20 wt% NFs with curing agents in the cores (i.e., they are composite self-healing materials). Therefore, the peak at 176.1 °C should also be present in the data for the matrices. The magnification of the DTG data for these matrices near 176.1 °C reveals weak peaks, confirming the presence of the curing agent in the composite material. The DTG data for the matrices near 305 °C are difficult to resolve because of the relatively small amount of PAN. Lastly, the boiling

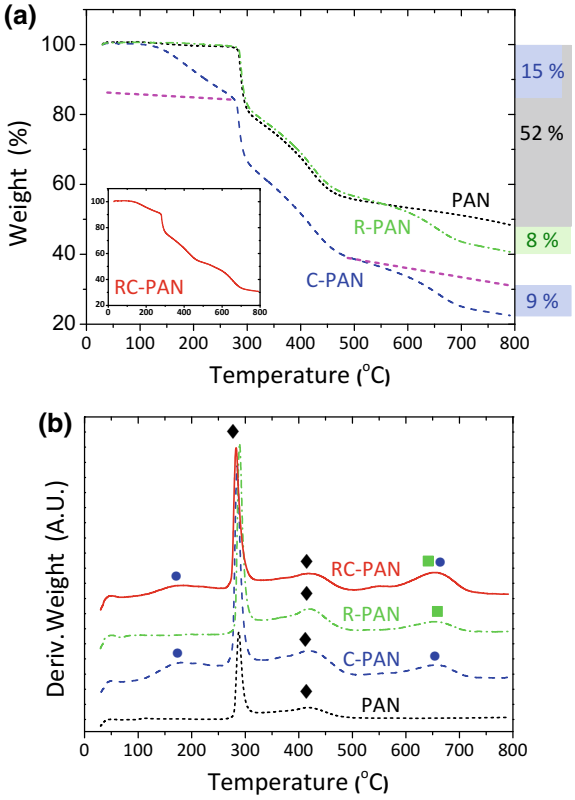

Fig. 5.12 Thermal analysis of PAN, R-PAN, C-PAN, and RC-PAN NFs. **a** TGA curves. The right-hand side column lists the total weight loss of the core and shell materials within the NFs (Gray: PAN, Green: resin monomer, Blue: curing agent; and purple line estimates the weight loss of curing agent). The insert graph shows the TGA results for RC-PAN NF mats. **b** DTG curves. The phase-transition temperatures of the core and shell materials are marked by black diamonds at 288 and 420 °C: PAN; green rectangles at 660 °C: resin monomer; blue circles at 180 and 660 °C: curing agent. The NF mats containing the resin monomer and curing agent in the fiber cores were obtained by co-electrospinning. Reprinted with permission from An et al. (2015)

temperature of the resin monomer in the matrices is 576.3 °C. At the resin monomer concentration of 5 wt%, the resin peak is indeterminate, with no distinctive peak, but rather a round peak. However, the resin monomer peak at 576.3 °C is clearly visible for the epoxy matrix containing 20 wt% of resin monomer.

The TGA was also conducted for NF mats with healing agents in the cores as formed using co-electrospinning (An et al. 2015; cf. Sect. 4.2). To determine the amount of the core or shell material contained in the NFs, TGA and DTG measurements are conducted, cf. Fig. 5.12. By comparing the TGA results (Fig. 5.12a) and the phase transition temperatures in the DTG results (Fig. 5.12b), the weight losses of the materials in question can be determined. In the temperature range of

0–800 °C, the weight losses of pristine PAN, curing agent, and resin monomer in the NFs are 52, 24, and 8%, respectively, consistent with the results of Lee et al. (2014a, b) discussed above. The weight loss of the curing agent was higher than that of the resin monomer because the volume of the resin monomer encapsulated in the resin-containing PAN (R-PAN) NFs is smaller than that of the curing agent encapsulated in the curing agent-containing PAN (C-PAN) NFs, since the resin monomer is mixed with n-hexane for stable co-electrospinning, as mentioned in Sect. 4.2. Because of the high evaporation rate of n-hexane, most of the n-hexane is evaporated before the samples are prepared for thermal analysis. Therefore, n-hexane is not detected in the TGA results, with no weight loss corresponding to n-hexane detected (not shown here). Figure 5.12 also shows the results for the mutually entangled R-PAN and C-PAN NF mats, which are denoted as RC-PAN NFs. It is instructive to see the differences in the phase-transition temperatures of the core and shell materials in NFs formed by different methods (cf. Figs. 5.10 and 5.11 with Fig. 5.12).

References

An S, Joshi BN, Lee MW, Kim NY, Yoon SS (2014) Electrospun graphene-ZnO nanofiber mats for photocatalysis applications. Appl Surf Sci 294:24–28

An S, Liou M, Song KY, Jo HS, Lee MW, Al-Deyab SS, Yarin AL, Yoon SS (2015) Highly flexible transparent self-healing composite based on electrospun core–shell nanofibers produced by coaxial electrospinning for anti-corrosion and electrical insulation. Nanoscale 7:17778–17785

Bleay SM, Loader CB, Hawyes VJ, Humberstone L, Curtis PT (2001) A smart repair system for polymer matrix composites. Compos A 32:1767–1776

Colthup NB, Daly LH, Wiberley SE (1975) Introduction to infrared and Raman spectroscopy, 3rd edn. Academic Press, New York

Farquharson S, Smith W, Rose J, Shaw M (2002) Correlations between molecular (Raman) and macroscopic (rheology) data for process monitoring of thermoset composite. J Process Anal Chem 7:45–53

Ghosal A, Sinha-Ray S, Sinha-Ray S, Yarin AL, Pourdeyhimi B (2016) Numerical modeling and experimental study of solution-blown nonwovens formed on a rotating drum. Polymer 105:255–263

Jayes L, Hard AP, Sene C, Parker SF, Jayasooriya UA (2003) Vibrational spectroscopic analysis of silicones: a Fourier transform-Raman and inelastic neutron scattering investigation. Anal Chem 75:742–746

Lee MW, An S, Jo HS, Yoon SS, Yarin AL (2015) Self-healing nanofiber-reinforced polymer composites: 1. Tensile testing and recovery of mechanical properties. ACS Appl Mater Interfaces 7:19546–19554

Lee MW, An S, Lee C, Liou M, Yarin AL, Yoon SS (2014a) Self-healing transparent core–shell nanofiber coatings for anti-corrosive protection. J Mater Chem A 2:7045–7053

Lee MW, An S, Lee C, Liou M, Yarin AL, Yoon SS (2014b) Hybrid self-healing matrix using core–shell nanofibers and capsuleless microdroplets. ACS Appl Mater Interfaces 6:10461–10468

Lee MW, Sett S, An S, Yoon SS, Yarin AL (2017a) Self-healing nano-textured vascular-like materials: Mode I crack propagation. ACS Appl Mater Interfaces 9:27223–27231

Lee MW, Yoon SS, Yarin AL (2017b) Release of self-healing agents in a material: What happens next? ACS Appl Mater Interfaces 9:17449–17455

Maiti NC, Apetri MM, Zagorski MG, Carey PR, Anderson VE (2004) Raman spectroscopic characterization of secondary structure in natively unfolded proteins: a-Synuclein. J Am Chem Soc 126:2399–2408

Merad L, Cochez M, Margueron S, Jauchem F, Ferriol M, Benyoucef B, Bourson P (2009) In-situ monitoring of the curing of epoxy resins by Raman spectroscopy. Polym Test 28:42–45

Pang JWC, Bond IP (2005a) 'Bleeding composites'—damage detection and self-repair using a biomimetic approach. Compos A 36:183–188

Pang JWC, Bond IP (2005b) A hollow fibre reinforced polymer composite encompassing self-healing and enhanced damage visibility. Compos Sci Technol 65:1791–1799

Patrick JF, Hart KR, Krull BP, Diesendruck CE, Moore JS, White SR, Sottos NR (2014) Continuous self-healing life cycle in vascularized structural composites. Adv Mater 26:4302–4308

Sett S, Lee MW, Weith M, Pourdeyhimi B, Yarin AL (2015) Biodegradable and biocompatible soy protein/polymer/adhesive sticky nano-textured interfacial membranes for prevention of Esca fungi invasion into pruning cuts and wounds of vines. J Mater Chem B 3:2147–2162

Sinha-Ray S, Lee MW, Sinha-Ray S, An S, Pourdeyhimi B, Yoon SS, Yarin AL (2013) Supersonic nanoblowing: a new ultra-stiff phase of nylon 6 in 20–50 nm confinement. J Mater Chem C 1:3491–3498

Sinha-Ray S, Pelot DD, Zhou ZP, Rahman A, Wu X-F, Yarin AL (2012) Encapsulation of self-healing materials by coelectrospinning, emulsion electrospinning, solution blowing and intercalation. J Mater Chem 22:9138–9146

Sinha-Ray S, Zhang Y, Yarin AL, Davis SC, Pourdeyhimi B (2011) Solution blowing of soy protein fibers. Biomacromol 12:2357–2363

Yerro O, Radojevic V, Radovic I, Petrovic M, Uskokovic PS, Stojanovic DB, Aleksic R (2016) Thermoplastic acrylic resin with self-healing properties. Polym Eng Sci 56:251–257

Zanjani JSM, Okan BS, Letofsky-Papst I, Menceloglu Y, Yildiz M (2015) Repeated self-healing of nano and micro scale cracks in epoxy based composites by tri-axial electrospun fibers including different healing agents. RSC Adv 5:73133–73145

Zanjani JSM, Okan BS, Yilmaz C, Menceloglu Y, Yildiz M (2017) Monitoring the interface and bulk self-healing capability of triaxial electrospun fibers in glass fiber reinforced epoxy composites. Compos A 99:221–232